HHS Public Access

Author manuscript

Sci Immunol. Author manuscript; available in PMC 2018 January 19.

Published in final edited form as:

Sci Immunol. 2017 November 17; 2(17): . doi:10.1126/sciimmunol.aan4631.

Suppression of FIP200 and autophagy by tumor-derived lactate promotes naïve T cell apoptosis and affects tumor immunity

Houjun Xia[1,*], **Wei Wang**[1,2,*], **Joel Crespo**[1,3], **Ilona Kryczek**[1,3], **Wei Li**[1], **Shuang Wei**[1], **Zhaoqun Bian**[1,4], **Tomasz Maj**[1], **Mingxiao He**[5], **Rebecca J. Liu**[6], **Youwen He**[5], **Ramandeep Rattan**[7], **Adnan Munkarah**[7], **Jun-Lin Guan**[8], and **Weiping Zou**[1,3,9,10,11,†]

[1]Department of Surgery, University of Michigan School of Medicine, Ann Arbor, MI 48109, USA

[2]Department of Immunology and Key Laboratory of Medical Immunology of Ministry of Public Health, Peking University Health Science Center, Beijing 100191, China

[3]Graduate Program in Immunology, University of Michigan School of Medicine, Ann Arbor, MI 48109, USA

[4]Department of Environmental Health, Cincinnati University College of Medicine, Cincinnati, OH 45267, USA

[5]Department of Immunology, School of Medicine, Duke University, Durham, NC 27710, USA

[6]Department of Obstetrics and Gynecology, University of Michigan School of Medicine, Ann Arbor, MI 48109, USA

[7]Department of Women's Health Services, Henry Ford Health System, Detroit, MI 48202, USA

[8]Department of Cancer Biology, Cincinnati University College of Medicine, Cincinnati, OH 45267, USA

[9]Department of Pathology, University of Michigan School of Medicine, Ann Arbor, MI 48109, USA

[10]Graduate Program in Tumor Biology, University of Michigan School of Medicine, Ann Arbor, MI 48109, USA

[11]University of Michigan Comprehensive Cancer Center, University of Michigan School of Medicine, Ann Arbor, MI 48109, USA

Abstract

Naïve T cells are poorly studied in cancer patients. We report that naïve T cells are prone to undergo apoptosis due to a selective loss of FAK family–interacting protein of 200 kDa (FIP200)

[†]Corresponding author. wzou@med.umich.edu.
[*]These authors contributed equally to this work.

SUPPLEMENTARY MATERIALS

immunology.sciencemag.org/cgi/content/full/2/17/eaan4631/DC1

Author contributions: H.X., W.W., I.K., and W.Z. designed the experiments and wrote the paper. H.X., W.W., I.K., J.C., W.L., T.M., and S.W. performed the experiments. Z.B. and J.-L.G. generated the *Fip200*$^{flox/flox}$ mice and reviewed the paper. M.H. and Y.H. provided the *Atg3*$^{flox/flox}$ mice. R.J.L., R.R., and A.M. provided clinical samples and information. H.X. and T.M. performed the statistical analysis.

Competing interests: The authors declare that they have no competing interests.

in ovarian cancer patients and tumor-bearing mice. This results in poor antitumor immunity via autophagy deficiency, mitochondria overactivation, and high reactive oxygen species production in T cells. Mechanistically, loss of FIP200 disables the balance between proapoptotic and antiapoptotic Bcl-2 family members via enhanced argonaute 2 (Ago2) degradation, reduced Ago2 and microRNA1198-5p complex formation, less microRNA1198-5p maturation, and consequently abolished microRNA1198-5p–mediated repression on apoptotic gene *Bak1*. Bcl-2 overexpression and mitochondria complex I inhibition rescue T cell apoptosis and promoted tumor immunity. Tumor-derived lactate translationally inhibits FIP200 expression by down-regulating the nicotinamide adenine dinucleotide level while potentially up-regulating the inhibitory effect of adenylate-uridylate–rich elements within the 3′ untranslated region of *Fip200* mRNA. Thus, tumors metabolically target naïve T cells to evade immunity.

INTRODUCTION

Memory T cells are the main effector components of antitumor immunity in most cancer types. The phenotypic and functional heterogeneity of memory T cells in the human cancer environment have been the focus of recent studies (1, 2). Human tumors progress despite the presence of tumor-associated antigen (TAA)–specific memory and effector T cells. Different molecular and cellular mechanisms contribute to the failure of effector T cells to eradicate the tumor. These include immunosuppressive networks that impair and suppress ongoing memory T cell function (3–5). Recent studies have shown that the metabolic alteration in the cancer microenvironment can directly mediate memory and effector T cell dysfunction (6, 7) and indirectly target antigen-presenting cells, particularly dendritic cells, to additionally impair effector T cell–mediated antitumor immunity (8). Memory T cells are differentiated from naïve T cells. There is a balanced loss and replacement of naïve T cells in the periphery (9). The molecular basis of naïve T cell quiescence has been studied in homeostasis in mice (10, 11). However, the nature of naïve T cells is poorly defined in patients with cancer and in tumor-bearing mouse models. Alteration of naïve T cells may likely affect T cell homeostasis and memory T cell differentiation and functionality in the tumor-bearing hosts. Here, we have studied the functional and molecular features of naïve T cells in patients with ovarian cancer and in several tumor-bearing mouse models. We have found that naïve T cells are prone to undergo apoptosis with an inhibition of FAK family–interacting protein of 200 kDa (FIP200; also known as RB1CC1) in cancer patients and tumor-bearing mice. Furthermore, we have determined that FIP200 inhibition contributed to naïve T cell apoptosis in tumor-bearing hosts and have elucidated the cellular and molecular mechanisms by which tumor-derived metabolite lactate selectively inhibits FIP200 expression, and FIP200 loss results in naïve T cell autophagy deficiency, apoptosis, and poor antitumor immunity.

RESULTS

FIP200 loss links to poor autophagy and high apoptosis in naïve T cells in tumor

Effector T cells are functionally impaired in the tumor microenvironment (2). However, naïve T cells are poorly examined in patients with cancer. We studied $CD45RO^{-}CD45RA^{+}CCR7^{+}CD62L^{+}CD7^{+}CD3^{+}$ naïve T cells in patients with ovarian cancer and in healthy

humans (Fig. 1A and fig. S1A). In addition to peripheral blood, $CD4^+$ and $CD8^+$ T cells with naïve phenotype existed in the ovarian cancer tissues (Fig. 1A). Naïve T cells exhibited higher amounts of spontaneous apoptosis in peripheral blood, cancer tissues (Fig. 1, B to D), and cancer ascites (fig. S1B) in ovarian cancer patients compared with healthy humans as shown by Annexin V^+ staining (Fig. 1, B to D, and fig. S1B) and cleaved caspase 3 expression (fig. S1C). After T cell receptor (TCR) engagement, there were also higher levels of apoptosis in peripheral blood naïve T cells from ovarian cancer patients compared with healthy humans (Fig. 1E). Similarly, increased spontaneous apoptosis was detected in mouse $CD3^+CD62L^+CD44^{low}$ naïve T cells in ID8 ovarian cancer–bearing mice as compared with normal mice (Fig. 1F). After TCR engagement, there were higher amounts of apoptotic naïve T cells in ID8 ovarian cancer–bearing mice than in controls (Fig. 1G).

Autophagy regulates cell survival and apoptosis (12, 13). To explore the mechanism by which naïve T cells are apoptotic in tumor-bearing hosts, we evaluated the expression of autophagy components and autophagy formation in naïve T cells in patients with ovarian cancer. We observed that the levels of FIP200 protein (Fig. 1H) were reduced in naïve T cells in patients with ovarian cancer as compared with that in healthy humans. Other autophagy components, including Atg3 and Atg5 in naïve T cells, were similar between ovarian cancer patients and healthy humans (Fig. 1H). The levels of FIP200 protein expression in memory T cells were comparable between ovarian cancer patients and healthy humans (fig. S1D). FIP200 is required for autophagosome formation (14). Thus, tumors may impair naïve T cell autophagy induction via altering FIP200 expression. In support of this possibility, we found that the expression of microtubule-associated protein 1A/1B light chain 3 (LC3), the marker of autophagosome formation, decreased in naïve T cells in patients with ovarian cancer as compared with that in healthy humans (Fig. 1H). To determine whether reduced autophagy was due to impaired induction or enhanced degradation of autophagosomes, we treated human naïve T cells with bafilomycin A (Baf), an inhibitor of autophagy degradation, and detected LC3-II. Baf treatment resulted in greater accumulation of LC3-II in naïve T cells from healthy humans compared with ovarian cancer patients (fig. S1E). Thus, tumors may selectively target FIP200 and predominantly impair autophagy formation in naïve T cells in patients with cancer.

We extended our patient studies to two tumor-bearing mouse models, ID8 ovarian cancer and LLC (Lewis lung carcinoma) lung cancer. In line with human studies, we found that the amounts of FIP200 protein and LC3-II were reduced in naïve T cells in tumor-bearing mice as compared with normal mice (Fig. 1I). Other autophagy components, including Atg3 and Atg5, were not consistently altered in naïve T cells in tumor-bearing mice as compared with normal mice (Fig. 1I). Thus, the results demonstrate a selective loss of FIP200, an impaired autophagy induction, and high apoptosis in naïve T cells in both cancer patients and tumor-bearing mice.

Genetic FIP200 deletion impairs autophagy induction and causes T cell apoptosis

Spontaneous loss of FIP200 impaired autophagy formation and was linked to naïve T cell apoptosis in tumor-bearing hosts (Fig. 1). We hypothesized that a loss of FIP200 resulted in naïve T cell apoptosis. To test this hypothesis, we crossed loxP-flanked *Fip200* alleles

(*Fip200*$^{flox/flox}$) mice (15) with mice with transgenic expression of Cre recombinase from the CD4 promoter to delete the loxP-flanked *Fip200* alleles specifically in T cells (called "*Fip200*$^{-/-}$ mice" here). As expected, we detected FIP200 expression in non–T cells but not in CD4$^+$ and CD8$^+$ T cells (Fig. 2A). Despite the deletion of *Fip200* in T cells, *Fip200*$^{-/-}$ mice had similar numbers of total thymocytes as well as CD4$^-$CD8$^-$, CD4$^+$CD8$^+$, CD4$^+$CD8$^-$, and CD4$^-$CD8$^+$ subsets with wild-type (WT) mice (fig. S2A). It suggests that FIP200 deficiency does not impair T cell development.

Next, we examined peripheral T cells in *Fip200*$^{-/-}$ mice. We found that naïve T cells in lymph nodes (Fig. 2, B and C) and spleen (fig. S2B) experienced higher levels of spontaneous apoptosis in *Fip200*$^{-/-}$ mice than in WT mice as shown by Annexin V and 7-amino actinomycin D (7AAD) staining. As a confirmation, we showed that *Fip200*$^{-/-}$ naïve T cells expressed elevated cleaved caspase 3 expression as shown by fluorescence-activated cell sorting (FACS; fig. S2C) and Western blotting (fig. S2D). Twenty-four and 48 hours after in vitro culture without (Fig. 2D and fig. S2C) and with (Fig. 2E and fig. S2C) TCR engagement, *Fip200*$^{-/-}$ naïve T cells exhibited increased apoptosis as compared with WT counterparts. Seventy-two hours after culture, 75 to 85% of *Fip200*$^{-/-}$ T cells became apoptotic compared with 35 to 45% of WT cells (fig.S2, E and F). As a result of peripheral T cell apoptosis, the percentage of T cell subsets was reduced in the lymph nodes, spleen, bone marrow, and peripheral blood in *Fip200*$^{-/-}$ mice compared with WT mice (Fig. 2F). Consistently, the absolute number of T cell subsets markedly decreased in the spleen (Fig. 2G) and lymph nodes (fig. S2G) of *Fip200*$^{-/-}$ mice compared with WT mice. Thus, FIP200 may intrinsically control T cell apoptosis. To further test this possibility, we adoptively transferred a mixture of equal numbers of CD45.1$^+$ WT and CD45.2$^+$ *Fip200*$^{-/-}$ donor T cells into *Rag1*$^{-/-}$ mice (fig. S2H). Fourteen days after transfusion, 90% CD4$^+$ and CD8$^+$ T cells were CD45.1$^+$ WT T cells (Fig. 2H). Again, high apoptosis was detected in CD45.2$^+$ *Fip200*$^{-/-}$ T cells rather than in CD45.1$^+$ WT T cells (Fig. 2I). Thus, loss of FIP200 results in T cell intrinsic apoptosis in vitro and in vivo. The data suggest that *Fip200*$^{-/-}$ T cells are functionally similar with naïve T cells in tumor-bearing hosts (Fig. 1). FIP200 is an autophagy component, and FIP200-mediated canonical autophagy is required to support neonatal survival and tumor cell growth (14, 16). In line with our observations in naïve T cells in human and mouse tumors (Fig. 1), we found reduced levels of LC3-II (Fig. 2J) and increased autophagy receptors, p62 and (nuclear dot protein 52) NDP52 (Fig. 2K), in *Fip200*$^{-/-}$ naïve T cells compared with WT naïve T cells. Thus, we further used *Fip200*$^{-/-}$ T cells in combination with T cells from tumor-bearing mice and patients with ovarian cancer to explore the mechanisms and functional features of FIP200-deficient T cells in tumor-bearing hosts.

FIP200 deficiency alters mitochondria activation and reactive oxygen species production in T cells

We studied the mechanisms by which FIP200 regulates T cell apoptosis. Mitochondria and reactive oxygen species (ROS) release are often associated with cell apoptosis (17, 18). We explored potential mitochondria abnormality in *Fip200*$^{-/-}$ T cells. MitoTracker analysis revealed an increase in mitochondria mass in *Fip200*$^{-/-}$ CD4$^+$ and CD8$^+$ T cells compared with WT cells (Fig. 3A). In line with these observations, we detected higher levels of ROS

(Fig. 3B), increased mitochondrial membrane potential (fig. S3A), and mitochondria-derived ROS (fig. S3B) in *Fip200*$^{-/-}$ T cells compared with WT T cells. Accordingly, knockdown of FIP200 (fig. S3C) in human naïve T cells resulted in increased ROS production (fig. S3D) and cell apoptosis (fig. S3E).

To determine whether FIP200 controls T cell apoptosis through altering mitochondria activity, we treated T cells with *N*-acetylcysteine (NAC) in vitro and analyzed T cell apoptosis. NAC can inhibit mitochondria function and target ROS production (19). NAC treatment had no effect on apoptosis of the WT primary (Fig. 3C) and activated (fig. S3F) CD4$^+$ and CD8$^+$ T cells. However, this treatment reduced apoptosis of primary (Fig. 3C) and activated (fig. S3F) *Fip200*$^{-/-}$ CD4$^+$ and *Fip200*$^{-/-}$ CD8$^+$ T cells. Next, we treated *Fip200*$^{-/-}$ mice with NAC in vivo and analyzed T cell apoptosis. NAC treatment caused marked reduction of Annexin V$^+$ *Fip200*$^{-/-}$ CD4$^+$ and Annexin V$^+$ *Fip200*$^{-/-}$ CD8$^+$ T cells (Fig. 3D). Further analysis revealed that NAC treatment predominantly rescued the naïve T cell compartment (Fig. 3E) and minimally increased memory T cells (fig. S3G). In addition, we treated the *Fip200*$^{-/-}$ and WT mice with another antioxidant, metformin, in vivo. Metformin is an inhibitor of mitochondria complex I and can reduce ROS levels (20). As expected, metformin reduced ROS expression (Fig. 3F) and apoptosis (Fig. 3G) in naïve T cells. Thus, *Fip200*$^{-/-}$ T cell apoptosis is linked to high mitochondria activity and ROS release in mice and humans. FIP200 may control T cell apoptosis via suppressing ROS production.

FIP200 deficiency impairs antitumor immunity

To investigate the role of FIP200 in T cell–mediated antitumor immunity, we inoculated MC38 colon cancer cells (Fig. 4, A and B) and B16 melanoma cells (Fig. 4, C and D) into the WT and *Fip200*$^{-/-}$ mice. We found that tumors were larger (Fig. 4, A and C) and heavier (Fig. 4, B and D) in *Fip200*$^{-/-}$ mice than in WT mice. Accordingly, there was less CD4$^+$ and CD8$^+$ T cell tumor infiltration in MC38 tumor-bearing *Fip200*$^{-/-}$ mice than in WT mice (Fig. 4E). To further confirm functional impairment of *Fip200*$^{-/-}$ naïve T cells, we transferred *Fip200*$^{-/-}$ and WT naïve T cells into *Rag1*$^{-/-}$ mice and established MC38 tumors as well as the colitis model (21). We found that CD45.2$^+$ *Fip200*$^{-/-}$ T cells expressed less interferon-γ (IFN-γ) in tumor-draining lymph nodes and tumor tissues compared with CD45.1$^+$ WT T cells (fig. S4A). In the colitis model, WT naïve T cells, but not *Fip200*$^{-/-}$ naïve T cells, induced severe colitis as shown by gradual body weight loss (fig. S4B). Thus, *Fip200*$^{-/-}$ T cells are functionally impaired.

Because FIP200 targets mitochondria, regulates ROS production, and affects T cell apoptosis and because manipulation of mitochondria activity with metformin treatment altered naïve T cell ROS expression and apoptosis (Fig. 3, F and G), we examined the potential effect of metformin on tumor progression and immune responses. We found that metformin treatment inhibited MC38 tumor growth in WT mice (Fig. 4, F and G). To investigate whether tumor growth inhibition was dependent on the immune response, we treated the MC38 tumor-bearing NSG-deficient mice with metformin. We observed that metformin treatment had no effect on tumor growth in the NSG mice (fig. S4, C and D). Furthermore, metformin treatment increased naïve T cells (fig. S4E) and reduced ROS expression in naïve T cells (Fig. 4H). Accordingly, the treatment resulted in decreased naïve

T cell apoptosis (Fig. 4, I and J). Thus, reduced FIP200 expression in naïve T cells impairs T cell function and T cell–mediated antitumor immunity.

FIP200 controls Bak expression via maintaining microRNA1198-5p expression

The cellular intrinsic apoptotic pathway is controlled by the balance of proapoptotic and antiapoptotic members of the Bcl-2 family (22). We examined whether the Bcl-2 family gene expression profile is altered in *Fip200*$^{-/-}$ mice. In line with this notion, we found that the expression of Bcl-2 was reduced in primary naïve *Fip200*$^{-/-}$ CD4^{+} and CD8^{+} naïve T cells as compared with WT naïve T cells (Fig. 5A). The expression levels of Bak and Bim, two proapoptotic Bcl-2 family members, were elevated in fresh naïve *Fip200*$^{-/-}$ CD4^{+} and CD8^{+} T cells as compared with WT T cells (Fig. 5B). Similar results were obtained in the cultured naïve T cell subsets without and with TCR engagement (fig. S5A). Thus, the imbalance between proapoptotic and apoptotic Bcl-2 family members may contribute to high apoptosis in *Fip200*$^{-/-}$ T cells.

To tilt this imbalance toward the antiapoptotic direction, we bred *Fip200*$^{-/-}$ mice with *Bcl-2* transgenic mice (10) and analyzed T cell apoptosis in *Fip200*$^{-/-}$ *Bcl-2* transgenic mice (fig. S5B). As expected, naïve T cell apoptosis was partially reduced in *Fip200*$^{-/-}$ *Bcl-2* transgenic mice compared with *Fip200*$^{-/-}$ mice (Fig. 5C). Consistently, *Fip200*$^{-/-}$ *Bcl-2* transgenic mice showed reduced apoptosis in naïve T cells without (fig. S5C) or with (fig. S5D) TCR engagements at different time points compared with *Fip200*$^{-/-}$ mice. In vivo Bcl-2 overexpression partially recovered CD4^{+} and CD8^{+} T cell numbers in the spleen (Fig. 5D) and lymph nodes (fig. S5E) in *Fip200*$^{-/-}$ mice. Thus, loss of FIP200 results in the imbalance between proapoptotic and antiapoptotic genes of Bcl-2 family members and contributes to naïve T cell intrinsic apoptosis.

MicroRNAs contribute to the maintenance of naïve T cell identity (23). We hypothesized that loss of FIP200 may be associated with the alteration of microRNA profiles in T cells. We conducted the microRNA arrays in *Fip200*$^{-/-}$ and WT naïve CD4^{+} T cells (table S1). Forty-two and 32 microRNAs were altered more than 25% in two sets of *Fip200*$^{-/-}$ naïve CD4^{+} T cells compared with that of WT (Fig. 5E). We searched for potential microRNAs, which can target Bcl-2 family genes via several microRNA bioinformatics tools, including miRWalk, TargetScan, and microRNA.org (fig. S5F). Among 42 decreased microRNAs, 10 microRNAs were predicted to potentially target proapoptotic genes *Bak1* and *Bcl2l11*. Among these 10 microRNAs, the levels of microRNA1198-5p, microRNA139- 3p, and microRNA342-5p were decreased by 18.9-, 12.9-, and 4.7-fold, respectively, in *Fip200*$^{-/-}$ T cells in the microRNA arrays (Fig. 5E). We quantified these three microRNAs in naïve *Fip200*$^{-/-}$ and WT CD4^{+} T cells (Fig. 5F) and confirmed that the microRNA1198-5p was the most reduced microRNA in naïve *Fip200*$^{-/-}$ CD4^{+} T cells compared with WT CD4^{+} T cells (Fig. 5F). The microRNA bioinformatics tools predicted that the 3′ untranslated region (3′UTR) of *Bak1* contains a defined target site of microRNA1198-5p (fig. S5G). To validate this target, we constructed a luciferase reporter construct containing the predicted 3′UTR of *Bak1* and a mutant vector containing the site mutations at the predicted targeting site (fig. S5G). Transfection of microRNA1198-5p mimics decreased the reporter activity of the WT 3′UTR-*Bak1* but not the mutant 3′UTR-*Bak1* (Fig. 5G). Furthermore, the inhibitors of

microRNA1198-5p increased the Bak expression in WT T cells, and its mimics decreased the Bak expression in *Fip200*$^{-/-}$ T cells compared with controls (Fig. 5H). However, other Bcl-2 family genes including *Bcl2l11* (Bim) and *BBC3* (PUMA) were not affected by the inhibitors or mimics of microRNA1198-5p (Fig. 5H). The data suggest that FIP200 deficiency may result in reduced microRNA1198-5p expression and lift the repression of microRNA1198-5p on Bak expression and consequently contributes to the increase in T cell apoptosis.

FIP200 maintains microRNA1198-5p expression via Ago2 in naïve T cells

We attempted to understand why there was a substantial loss of microRNA1198-5p in *Fip200*$^{-/-}$ T cells. The microRNA-induced silencing complex (miRISC) controls the maturation of microRNAs (24). Argonaute 2 (Ago2), Drosha, and Dicer are the core components of miRISC (*25*). Western blotting revealed a decrease of Ago2 expression (Fig. 6A) but not of Drosha and Dicer expression (fig. S6A) in *Fip200*$^{-/-}$ naïve T cells. We hypothesized that FIP200 affected Ago2 expression and, subsequently, microRNA1198-5p expression in T cells. We knocked down the Ago2 expression with specific small interfering RNAs (siRNAs) in WT naïve T cells (fig. S6B). As expected, siRNA against Ago2 resulted in decreased microRNA1198-5p expression but not microRNA342-5p expression (Fig. 6B). Thus, the data suggest that FIP200 deficiency results in reduced Ago2 expression and abolishes microRNA1198-5p expression in T cells.

Substantial microRNAs were altered in *Fip200*$^{-/-}$ T cells (Fig. 5E). Next, we explored why there was a relatively selective loss of microRNA1198-5p expression in *Fip200*$^{-/-}$ T cells. We wondered whether microRNA1198-5p and Ago2 formed a complex and FIP200 deletion impaired the complex formation in naïve T cells. To this end, we pulled down the Ago2 protein from WT T cells (fig. S6C) and found that microRNA1198-5p and microRNA342-5p, but not microRNA325-5p, were highly associated with Ago2 protein (Fig. 6C). MicroRNA325-5p expression was not affected by FIP200 deficiency in T cells (Fig. 5E). *Bak1* and *Bax* mRNAs, but not *Bcl2l11* and *Bbc3* mRNAs, were also found in the pulled down Ago2 complexes in WT T cells (Fig. 6D). However, the content of *Bak1*, but not *Bax* mRNA, in the Ago2 complexes, was reduced sixfold in *Fip200*$^{-/-}$ naïve T cells compared with WT T cells (Fig. 6E). It suggests that Ago2 failed to associate with and repress *Bak1* mRNA expression via microRNA1198-5p expression in FIP200-deficient naïve T cells. Thus, Ago2, microRNA1198- 5p, and *Bak1* mRNA form a complex in naïve T cells, and FIP200 deletion impairs the complex and consequently leads to high *Bak1* expression in naïve T cells.

Next, we investigated how Ago2 expression was reduced in *Fip200*$^{-/-}$T cells. Ago2 transcripts were comparable in *Fip200*$^{-/-}$ and WT naïve CD4^{+} and CD8^{+} T cells (fig. S6D). Ago2 may be ubiquitinated and degraded in the proteasome (23). To test this possibility, we treated naïve T cells with MG132 and performed immunoprecipitation assays with anti-Ago2 antibody (fig. S6E). Ubiquitin immunoblotting demonstrated that MG132 treatment had no effect on Ago2 ubiquintination in WT T cells but resulted in high amounts of ubiquintinated Ago2 (Ub-Ago2) in *Fip200*$^{-/-}$ T cells (Fig. 6F). Unfortunately, the only reported E3 of Ago2, named Trim71, was not expressed in T cells (23). We wondered

whether the decrease of Ago2 was exclusively attributed to the FIP200 depletion among the autophagy components. We checked the Ago2 expression in *Atg3* knockout (*Atg3*-KO) T cells (26). Similar to *Fip200*$^{-/-}$ T cells, we detected reduced Ago2 and enhanced Bak expression in *Atg3*-KO naïve T cells (Fig. 6G). The data suggest that the interplay between Ago2 and autophagy pathway may collaboratively regulate T cell apoptosis. Thus, FIP200 maintains microRNA1198-5p expression via Ago2 in naïve T cells and regulates T cell survival by controlling the mitochondria mass and ROS production.

Tumor-derived lactate suppresses FIP200 expression in naïve T cells

We next studied whether and how tumor cells may metabolically lead to the down-regulation of FIP200 in naïve T cells. It is thought that interaction between autophagy and mitochondria may dictate cell fate in response to metabolic fluctuations (27). Although there are naïve T cells in the tumor site, naïve T cells are predominantly located in the secondary lymphoid organs and peripheral blood. We assume that tumor-secreted factor(s) systemically targets FIP200 in naïve T cells. Aerobic glycolysis is a feature of cancer cell metabolism. Under aerobic glycolysis, cancer cells produce lactates. We hypothesized that tumor-derived lactate inhibits FIP200 expression and causes T cell apoptosis. We treated human naïve T cells with different concentrations of lactate. We found that treatment with lactate led to reduced FIP200 (Fig. 7A) and LC-3II (fig. S7A) expression and increased apoptosis (Fig. 7B) in human naïve T cells. Other autophagy components—including Atg3, Atg5, and Beclin1—were not altered (fig. S7A).

We measured lactate in plasma and ascites fluids from patients with ovarian cancer. Lactate plasma levels were less than 2.2 mM in healthy individuals (28). Elevated lactate levels in plasma and ascites were detected in patients with ovarian cancer (Fig. 7C). We treated human naïve T cell with 0 to 20% ovarian cancer ascites. We found that ascites caused reduced FIP200 and LC3-II expression in T cells (Fig. 7D). Ascites had no effect on other autophagy components (fig. S7B). α-Cyano-4-hydroxycinnamate (CHC), a monocarboxylate channel transporter inhibitor, can inhibit lactate uptake (29). Addition of CHC partially rescued the suppressed FIP200 expression by lactate or ascites (Fig. 7E). Similarly, treatment with lactate resulted in decreased expression of FIP200 and Ago2 (Fig. 7F) and increased expression of Bak (Fig. 7F) and ROS production (Fig. 7G) in mouse naïve T cells.

Next, we studied the mechanism by which lactate repressed the FIP200 expression in naïve T cells. Treatment with lactate did not change *Fip200* mRNA expression in mouse naïve T cells (fig. S7C). Furthermore, the protease inhibitor MG132 did not alter the expression of FIP200 protein in the presence of lactate in mouse naïve T cells (fig. S7D). It suggests that lactate may inhibit FIP200 expression via a posttranscriptional regulation. The adenylate-uridylate–rich elements (AREs) in 3′UTR are often the targets of the RNA-binding proteins and affect protein turnover as *cis* elements (30). We found seven “AUUUA” pentamer AREs within the mouse *Fip200* 3′UTR (fig. S7E). To determine whether such AREs are critical for reduced FIP200 expression in lactate-treated naïve T cells, we constructed a firefly luciferase reporter plasmid by inserting the 3′UTR containing the front six AREs of mouse *Fip200*. The control plasmid expressed the mutated *Fip200* 3′UTR by replacing the AREs

with a “CGCGG” sequence. The mutant 3′UTR reporter showed an increase ratio of Firefly/*Renilla* luciferase activity compared with the WT 3′UTR of mouse *Fip200* (Fig. 7H). The result indicated that the AREs within 3′UTR are critical for the down-regulation of mouse *Fip200* expression. Nicotinamide adenine dinucleotide (NAD) up-regulates IFN-γ expression by inhibiting glyceraldehyde-3- phosphate dehydrogenase (GAPDH) binding to the AREs of the IFN-γ mRNA (31). We hypothesized that lactate might repress the FIP200 expression through down-regulating the NAD level in naïve T cells. In support of this possibility, treatment with lactate caused a decrease in the total NAD level in naïve T cells (Fig. 7I). Nicotinamide (NAM), a precursor of NAD, increased the total NAD level (fig. S7F) and up-regulated the FIP200 protein (Fig. 7J), but not *Fip200* mRNA (fig. S7G), expression in naïve T cells treated with lactate. Accordingly, treatment with NAM resulted in a reduced inhibitory effect on luciferase activity via the AREs within the 3′UTR of mouse *Fip200* (Fig. 7K). The data suggest that NAD may affect the functional activity of the AREs of *Fip200*. In further support of this, treatment with NAM reduced naïve T cell apoptosis induced by lactate (Fig. 7L). Thus, biochemically, tumor-derived lactate reduces the NAD level, may offer more dehydrogenases binding within the AREs of *Fip200* mRNA, and reduces FIP200 protein expression. Functionally, tumor-derived lactate-mediated FIP200 reduction leads to autophagy malformation and mitochondria overactivation. On the one hand, autophagy malformation enhances *Bak1* expression via increased Ago2 degradation and reduced microRNA1198-5p expression and promotes T cell apoptosis. On the other hand, it has been defined that autophagy malformation–associated mitochondria overactivation inhibits Bcl-2 expression via ROS production (26, 32–34) and sensitizes T cell apoptosis (35). Therefore, tumor metabolism alters FIP200 expression and controls naïve T cell apoptosis by disabling the balance between proapoptotic (e.g., Bak1) and antiapoptotic (e.g., Bcl-2) gene expression (fig. S7H).

DISCUSSION

Naïve T cells are poorly studied in patients with cancer. Here, we have found that naïve T cells are prone to undergo apoptosis and lose quiescence and that FIP200 plays a key role in the regulation of naïve T cell apoptosis in patients with cancer and in several tumor-bearing mouse models.

FIP200 is essential for mammal autophagosome initiation (14). The role of FIP200 has been studied in different types of nonimmune cells (36, 37). The involvement of tumor-associated autophagy components in chemotherapy-induced antitumor immunity has been reported in tumor-bearing mouse models (38). However, the expression and biological activity of FIP200 in T cells (including human T cells) have not been studied. We have found that FIP200 expression, but not other typical autophagy components, is selectively reduced in naïve T cells in tumor-bearing mouse models and in patients with cancer. FIP200-deficient naïve T cells are highly susceptible to becoming apoptotic and mediate poor tumor immunity. Thus, in addition to malfunction of memory T cells (2), naïve T cell homeostasis is altered in tumor-bearing hosts. Furthermore, naïve T cell dysfunction may likely affect de novo priming of T cells recognizing neoantigens (39) and other TAAs accumulating throughout tumor progression and/or in the course of different types of cancer therapy, including immunotherapy, radiation therapy, and chemotherapy (40, 41). Thus, abnormal

naïve T cell biology may result in impaired effector T cell–mediated antitumor immunity and unfavorable therapeutic outcome in patients with cancer.

We assume a causal relationship between FIP200 loss and naïve T cell apoptosis. In support of this possibility, genetic deletion of FIP200 in T cells results in autophagy deficiency, followed by accumulated mitochondria content and excess amounts of ROS production and increased apoptosis in both mouse and human naïve T cells. Naïve T cells in both tumor-bearing mice and ovarian cancer patients mirror the phenotype and function of FIP200-deficient T cells. Furthermore, blocking ROS expression partially prevents *Fip200*$^{-/-}$ naïve T cells and tumor-associated WT naïve T cells from apoptosis and improves antitumor immunity. Thus, loss of FIP200 in naïve T cells targets mitochondria and promotes T cell apoptosis partially in an ROS-dependent manner.

It is well known that the Bcl-2 family members regulate mitochondria-associated cell apoptosis (13, 42). We have detected reduced expression of an antiapoptotic member, Bcl-2, and increased expression of proapoptotic members, Bak and Bim, in *Fip200*$^{-/-}$ naïve T cells. To examine the functional importance of this imbalance of the Bcl-2 family members, we have introduced the Bcl-2 transgene into FIP200-deficient T cells. We have found that the Bcl-2 transgene can partially rescue *Fip200*$^{-/-}$ T cell apoptosis. Therefore, loss of FIP200 in naïve T cells results in the imbalance between proapoptotic and antiapoptotic Bcl-2 family genes and contributes to *Fip200*$^{-/-}$ T cell apoptosis and naïve T cell apoptosis in tumor-bearing hosts. Similar to our observation in *Fip200*$^{-/-}$ T cells, it has been reported that autophagy deficiency causes mitochondria overactivation and ROS production (26, 32–34) and that ROS can regulate Bcl-2 expression (35). Thus, we have focused our mechanistic studies on the molecular pathway, which promotes the proapoptotic gene expression in FIP200-deficient naïve T cells and in naïve T cell apoptosis in tumor-bearing hosts. MicroRNAs contribute to the maintenance of naïve T cell identity (23). Our microRNA array and bioinformatics analysis demonstrate a major loss of microRNA1198-5p in FIP200-deficient naïve T cells. We have revealed that microRNA1198-5p can target *Bak1* expression, and microRNA1198-5p and *Bak1* mRNA are colocalized in the Ago2-related miRISC in FIP200-proficient naïve T cells. This colocalization is lost in FIP200-deficient T cells. It suggests that the association of FIP200 and Ago2 facilitates the binding of microRNA1198-5p to *Bak1* mRNA within miRISC, leading to *Bak1* translational inhibition. Ago2 deficiency impairs microRNA biogenesis from precursor microRNAs in the hematopoietic cells (43). We reason that the decreased Ago2 expression explains the loss of microRNA1198-5p and subsequent increase in Bak expression and enhanced apoptosis in *Fip200*$^{-/-}$ naïve T cells and in naïve T cells in tumor-bearing hosts. Because we have detected enhanced Ago2 degradation and increased ROS production in both *Fip200*$^{-/-}$ and *Atg3*$^{-/-}$ naïve T cells, our results suggest a potential universal regulatory role of the autophagy pathway in controlling Ago2 stability and expression in T cells.

Because FIP200 loss defines naïve T cell apoptosis in tumor-bearing hosts, we have explored how tumors target T cell FIP200 expression. Many types of tumor metabolically rely on glycolysis to generate adenosine triphosphate, which is followed by lactic acid fermentation and lactate production (44). High levels of lactate can affect different immune cell subset functions (28, 29, 45). However, it is unknown whether and how tumor-derived

lactate affects human and mouse naïve T cell phenotype and function. We detect high levels of lactate in plasma and ascites of ovarian cancer patients. Tumor-derived lactate targets FIP200 but not other autophagy components in T cells. The AREs within the 3′UTR are often the targets of the RNA-binding proteins and affect specific protein turnover as *cis* elements (30). Because we have found seven ARE sites within the 3′UTR of *Fip200* mRNA, selective loss of FIP200 may be associated with its multiple ARE sites. This possibility is initially supported by the increased luciferase activity of the 3′UTR of *Fip200* mRNA with the mutated AREs compared with the WT cells. Furthermore, we have demonstrated that (i) lactate down-regulates the NAD level along with reduced FIP200 protein expression in naïve T cells; (ii) an NAD precursor, NAM, increases the NAD level as well as the FIP200 protein expression; and (iii) NAM reduces the inhibitory effect on luciferase activity via the AREs within 3′UTR of *Fip200* mRNA. Thus, lactate down-regulates the NAD level and may potentially release more NAD-binding dehydrogenases to bind with the AREs within 3′UTR of *Fip200* mRNA, and finally results in reduced FIP200 protein expression. Similar mechanisms are proposed in the literature. For example, GAPDH, as a NAD-binding protein, can regulate the expression of IFN-γ (31, 46), hypoxia-inducible factor 1α (47), and colony-stimulating factor 1 (48) by binding to their AREs within these mRNAs through the NAD-binding domain. Thus, we have suggested a previously unappreciated mechanism for tumor-derived lactate in the regulation of T cell–mediated tumor immunity: Tumor metabolically affects naïve T cell apoptosis and reduces T cell–mediated antitumor immunity via two intertwined events, autophagy deficiency and mitochondria activation. However, there are certain limitations in our study. For example, the molecular link between these two events and the mechanism of Ago2 degradation deserve additional investigations. In addition, substantial studies have been conducted in mice with specific FIP200 deficiency in the entire T cell population, including naïve and memory T cells. This mouse system may not fully recapitulate the phenotype of naïve T cells in patients with cancer.

In summary, naïve T cells are poorly investigated in patients with cancer. The demonstration that a selective loss of FIP200 is a molecular feature of naïve T cell dysfunction in tumor-bearing hosts provides an insight into tumor-immune evasion mechanisms. The identification that the molecular network of lactate and FIP200 is functionally linked to autophagy activity and apoptosis in naïve T cells is important for understanding naïve T cell homeostasis in tumor-bearing hosts. We suggest that apoptosis of naïve T cells is a barrier to effective spontaneous antitumor immunity and should be considered a critical factor in the development of cancer immunotherapies and that targeting this network may be meaningful to maintain a naïve T cell pool, sustain potent effector T cell antitumor immunity, and improve cancer immunotherapies.

MATERIALS AND METHODS

Study design

This study was designed to demonstrate whether and how tumor cells evade tumor immunity via metabolic regulation of naïve T cell apoptosis. Mouse models and ovarian cancer patients were research models in the work. Sample sizes were estimated on the basis of

previous studies. The number of biological replicates for each data point is included in the figure legends. No outliers were excluded.

Peripheral blood and cancer tissues

Patients with ovarian cancer were recruited for this study as we previously described (7, 49–52). Blood, ascites, and cancer tissues were collected from patients with informed consent according to the procedures approved by the Institutional Review Boards of the University of Michigan School of Medicine.

Mouse models

Six- to 8-week-old WT C57BL/6 mice (Harlan Laboratories), *Cd4*-Cre C57BL/6 mice (Taconic Biosciences), *Lck*-Cre C57BL/6 mice, floxed *Fip200* (*Fip200*$^{flox/flox}$) C57BL/6 mice (53), floxed *Atg3* (*Atg3*$^{flox/flox}$) C57BL/6 mice (26), and *Bcl-2* transgenic C57BL/6 mice (54) were used for this study. *Fip200*$^{flox/flox}$ mice ("WT" here) were intercrossed with *Cd4*-Cre mice to delete the loxP-flanked *Fip200* alleles specifically in T cells (named *Fip200*$^{-/-}$ mice or "KO" here), which were further intercrossed with *Bcl-2* transgenic mice for overexpressing human Bcl-2 in WT ("*Bcl-2*–WT" here) or *Fip200*$^{-/-}$ mice ("*Bcl-2*–KO" here). *Atg3*$^{flox/flox}$ mice ("*Atg3*-WT" here) were intercrossed with *Lck*-Cre mice to delete the loxP-flanked *Atg3* alleles specifically in T cells (named "*Atg3*-KO" here). All mice were bred in-house and maintained under specific pathogen–free conditions. All animal research performed was approved by the Committee on Use and Care of Animals at the University of Michigan. MC38 colon carcinoma cells, ID8 ovarian cancer cells, LLC cells, and B16 melanoma cells were used for this work. ID8 luciferase cells (2.5×10^5) were injected into the peritoneal cavity of WT mice. Tumor progression was monitored two times per week by Xenogen IVIS Spectrum in vivo bioluminescence imaging system (PerkinElmer). After 28 days, the mesenteric lymph nodes were used to isolate naïve T cells. LLC cells (8×10^5) were inoculated subcutaneously into WT mice, and the inguinal lymph nodes were used after 2 weeks. MC38 (6×10^5) or B16 (4×10^5) cells were inoculated subcutaneously into WT or *FIP200*$^{-/-}$ mice. Tumor size was measured every 3 days using calipers fitted with a Vernier scale. Tumor volume was calculated on the basis of three perpendicular measurements.

FACS and analysis

Human cells were stained with fluorescence-conjugated antibodies to CD3 (clone HIT3a), CD4 (clone RPA-T4), CD8 (clone RPA-T8), CD45RA (clone HI100), CD45RO (clone UCHL1), CD62L (clone DREG–56), CCR7 (clone 150503) (BD Biosciences), and CD7 (clone 124-1D1, eBioscience). T cell subsets were enriched by negative selection with a RosetteSep Human T Cell Enrichment Cocktail (StemCell Technologies) from peripheral blood and ovarian cancer tissues. Naïve T cells were obtained with CD45RO bead–negative selection (Miltenyi Biotec) and sorted and confirmed by FACS with 98% purity. Mouse single-cell suspensions were prepared from thymus, bone marrow, peripheral blood, lymph nodes, and spleen and labeled with fluorescence-conjugated antibodies to CD3 (clone 17A2), CD4 (clone RM4–5), CD8 (clone 53-6.7), CD19 (clone 1D3), CD44 (clone IM7), CD45.1 (clone A20), CD62L (MEL–14), CD90 (clone 53-2.1) (BD Biosciences), CD45.2 (clone 104), and CD45RB (clone C363.16A, eBioscience). Then, if necessary, the cells were

sorted (BD FACSAria) or acquired on an LSR II flow cytometer (BD Biosciences), and data were analyzed with DIVA software (BD Biosciences).

RNA extraction, reverse transcription, and real-time polymerase chain reaction

RNA extraction, reverse-transcription, and real-time polymerase chain reaction (PCR) were described previously (52). Primers are listed in table S2.

MicroRNA array

The total RNA of WT or *Fip200*$^{-/-}$ naïve CD4^{+} T cells was extracted using TRIzol Reagent. The RNAs were applied for microRNA profiling via the OpenArray system at the University of Michigan DNA Sequencing Core. The expression of microRNA was quantified by TaqMan MicroRNA Assay (Applied Biosystems).

Lactate quantification

Lactate was measured with a Lactate Assay Kit (Sigma-Aldrich) according to the manufacturer's instructions.

NAD/NADH quantification

The amount of total NAD in 1 million mouse naïve T cells was measured with the NAD/NADH (reduced form of NAD^{+}) quantification kit (Sigma-Aldrich) according to the manufacturer's instructions.

Statistical analysis

Mann-Whitney *U* test was used to compare two independent groups. Student's *t* test was used for paired samples. All analyses were done using SPSS 13.0 and GraphPad Prism 5 software. $P < 0.05$ was considered statistically significant.

Supplementary Material

Refer to Web version on PubMed Central for supplementary material.

Acknowledgments

We would like to thank L. Cabrera, D. Postiff, M. Vinco, R. Craig, and J. Barikdar at the University of Michigan for their assistance.

Funding: This work is supported in part by NIH grants (CA217510, CA123088, CA099985, CA156685, CA171306, CA190176, CA193136, and 5P30CA46592), the Ovarian Cancer Research Fund, and Marsha Rivkin Center for Ovarian Cancer Research.

References

1. Wherry EJ. T cell exhaustion. Nat. Immunol. 2011; 12:492–499. [PubMed: 21739672]
2. Crespo J, Sun H, Welling TH, Tian Z, Zou W. T cell anergy, exhaustion, senescence, and stemness in the tumor microenvironment. Curr. Opin. Immunol. 2013; 25:214–221. [PubMed: 23298609]
3. Zou W. Immunosuppressive networks in the tumour environment and their therapeutic relevance. Nat. Rev. Cancer. 2005; 5:263–274. [PubMed: 15776005]

4. Topalian SL, Drake CG, Pardoll DM. Immune checkpoint blockade: A common denominator approach to cancer therapy. Cancer Cell. 2015; 27:450–461. [PubMed: 25858804]
5. Stephen TL, Rutkowski MR, Allegrezza MJ, Perales-Puchalt A, Tesone AJ, Svoronos N, Nguyen JM, Sarmin F, Borowsky ME, Tchou J, Conejo-Garcia JR. Transforming growth factor β-mediated suppression of antitumor T cells requires FoxP1 transcription factor expression. Immunity. 2014; 41:427–439. [PubMed: 25238097]
6. Chang C-H, Qiu J, O'Sullivan D, Buck MD, Noguchi T, Curtis JD, Chen Q, Gindin M, Gubin MM, van der Windt GJW, Tonc E, Schreiber RD, Pearce EJ, Pearce EL. Metabolic competition in the tumor microenvironment is a driver of cancer progression. Cell. 2015; 162:1229–1241. [PubMed: 26321679]
7. Zhao E, Maj T, Kryczek I, Li W, Wu K, Zhao L, Wei S, Crespo J, Wan S, Vatan L, Szeliga W, Shao I, Wang Y, Liu Y, Varambally S, Chinnaiyan AM, Welling TH, Marquez V, Kotarski J, Wang H, Wang Z, Zhang Y, Liu R, Wang G, Zou W. Cancer mediates effector T cell dysfunction by targeting microRNAs and EZH2 via glycolysis restriction. Nat. Immunol. 2016; 17:95–103. [PubMed: 26523864]
8. Cubillos-Ruiz JR, Silberman PC, Rutkowski MR, Chopra S, Perales-Puchalt A, Song M, Zhang S, Bettigole SE, Gupta D, Holcomb K, Ellenson LH, Caputo T, Lee A-H, Conejo-Garcia JR, Glimcher LH. ER stress sensor XBP1 controls anti-tumor immunity by disrupting dendritic cell homeostasis. Cell. 2015; 161:1527–1538. [PubMed: 26073941]
9. Surh CD, Sprent J. Homeostasis of naive and memory T cells. Immunity. 2008; 29:848–862. [PubMed: 19100699]
10. Yang K, Neale G, Green DR, He W, Chi H. The tumor suppressor Tsc1 enforces quiescence of naive T cells to promote immune homeostasis and function. Nat. Immunol. 2011; 12:888–897. [PubMed: 21765414]
11. Yang K, Shrestha S, Zeng H, Karmaus PWF, Neale G, Vogel P, Guertin DA, Lamb RF, Chi H. T cell exit from quiescence and differentiation into T_H2 cells depend on Raptor-mTORC1–mediated metabolic reprogramming. Immunity. 2013; 39:1043–1056. [PubMed: 24315998]
12. Levine B, Mizushima N, Virgin HW. Autophagy in immunity and inflammation. Nature. 2011; 469:323–335. [PubMed: 21248839]
13. Mariño G, Niso-Santano M, Baehrecke EH, Kroemer G. Self-consumption: The interplay of autophagy and apoptosis. Nat. Rev. Mol. Cell Biol. 2014; 15:81–94. [PubMed: 24401948]
14. Hara T, Takamura A, Kishi C, Iemura S, Natsume T, Guan J-L, Mizushima N. FIP200, a ULK-interacting protein, is required for autophagosome formation in mammalian cells. J. Cell Biol. 2008; 181:497–510. [PubMed: 18443221]
15. Wei H, Gan B, Wu X, Guan J-L. Inactivation of FIP200 leads to inflammatory skin disorder, but not tumorigenesis, in conditional knock-out mouse models. J. Biol. Chem. 2009; 284:6004–6013. [PubMed: 19106106]
16. Mizushima N. Autophagy. FEBS Lett. 2010; 584:1279. [PubMed: 20184884]
17. Kroemer G, Galluzzi L, Brenner C. Mitochondrial membrane permeabilization in cell death. Physiol. Rev. 2007; 87:99–163. [PubMed: 17237344]
18. Green DR, Galluzzi L, Kroemer G. Mitochondria and the autophagy–inflammation–cell death axis in organismal aging. Science. 2011; 333:1109–1112. [PubMed: 21868666]
19. Zafarullah M, Li WQ, Sylvester J, Ahmad M. Molecular mechanisms of N-acetylcysteine actions. Cell. Mol. Life Sci. 2003; 60:6–20. [PubMed: 12613655]
20. Owen MR, Doran E, Halestrap AP. Evidence that metformin exerts its anti-diabetic effects through inhibition of complex 1 of the mitochondrial respiratory chain. Biochem. J. 2000; 348:607–614. [PubMed: 10839993]
21. Powrie F, Leach MW, Mauze S, Caddie LB, Coffman RL. Phenotypically distinct subsets of $CD4^+$ T cells induce or protect from chronic intestinal inflammation in C. B-17 scid mice. Int. Immunol. 1993; 5:1461–1471. [PubMed: 7903159]
22. Czabotar PE, Lessene G, Strasser A, Adams JM. Control of apoptosis by the BCL-2 protein family: Implications for physiology and therapy. Nat. Rev. Mol. Cell Biol. 2014; 15:49–63. [PubMed: 24355989]

23. Bronevetsky Y, Villarino AV, Eisley CJ, Barbeau R, Barczak AJ, Heinz GA, Kremmer E, Heissmeyer V, McManus MT, Erle DJ, Rao A, Ansel KM. T cell activation induces proteasomal degradation of Argonaute and rapid remodeling of the microRNA repertoire. J. Exp. Med. 2013; 210:417–432. [PubMed: 23382546]
24. Bushati N, Cohen SM. microRNA functions. Annu. Rev. Cell Dev. Biol. 2007; 23:175–205. [PubMed: 17506695]
25. Meister G. Argonaute proteins: Functional insights and emerging roles. Nat. Rev. Genet. 2013; 14:447–459. [PubMed: 23732335]
26. Jia W, He Y-W. Temporal regulation of intracellular organelle homeostasis in T lymphocytes by autophagy. J. Immunol. 2011; 186:5313–5322. [PubMed: 21421856]
27. Green DR, Galluzzi L, Kroemer G. Metabolic control of cell death. Science. 2014; 345:1250256. [PubMed: 25237106]
28. Fischer K, Hoffmann P, Voelkl S, Meidenbauer N, Ammer J, Edinger M, Gottfried E, Schwarz S, Rothe G, Hoves S, Renner K, Timischl B, Mackensen A, Kunz-Schughart L, Andreesen R, Krause SW, Kreutz M. Inhibitory effect of tumor cell–derived lactic acid on human T cells. Blood. 2007; 109:3812–3819. [PubMed: 17255361]
29. Colegio OR, Chu N-Q, Szabo AL, Chu T, Rhebergen AM, Jairam V, Cyrus N, Brokowski CE, Eisenbarth SC, Phillips GM, Cline GW, Phillips AJ, Medzhitov R. Functional polarization of tumour-associated macrophages by tumour-derived lactic acid. Nature. 2014; 513:559–563. [PubMed: 25043024]
30. Barreau C, Paillard L, Osborne HB. AU-rich elements and associated factors: Are there unifying principles? Nucleic Acids Res. 2005; 33:7138–7150. [PubMed: 16391004]
31. Nagy E, Rigby WFC. Glyceraldehyde-3-phosphate dehydrogenase selectively binds AU-rich RNA in the NAD^+-binding region (Rossmann fold). J. Biol. Chem. 1995; 270:2755–2763. [PubMed: 7531693]
32. Willinger T, Flavell RA. Canonical autophagy dependent on the class III phosphoinositide-3 kinase Vps34 is required for naive T-cell homeostasis. Proc. Natl. Acad. Sci. U.S.A. 2012; 109:8670–8675. [PubMed: 22592798]
33. Pua HH, Guo J, Komatsu M, He Y-W. Autophagy is essential for mitochondrial clearance in mature T lymphocytes. J. Immunol. 2009; 182:4046–4055. [PubMed: 19299702]
34. Stephenson LM, Miller BC, Ng A, Eisenberg J, Zhao Z, Cadwell K, Graham DB, Mizushima NN, Xavier R, Virgin HW, Swat W. Identification of *Atg5*-dependent transcriptional changes and increases in mitochondrial mass in *Atg5*-deficient T lymphocytes. Autophagy. 2009; 5:625–635. [PubMed: 19276668]
35. Hildeman DA, Mitchell T, Aronow B, Wojciechowski S, Kappler J, Marrack P. Control of *Bcl-2* expression by reactive oxygen species. Proc. Natl. Acad. Sci. U.S.A. 2003; 100:15035–15040. [PubMed: 14657380]
36. Wei H, Wei S, Gan B, Peng X, Zou W, Guan J-L. Suppression of autophagy by FIP200 deletion inhibits mammary tumorigenesis. Genes Dev. 2011; 25:1510–1527. [PubMed: 21764854]
37. Wang C, Liang C-C, Bian ZC, Zhu Y, Guan J-L. FIP200 is required for maintenance and differentiation of postnatal neural stem cells. Nat. Neurosci. 2013; 16:532–542. [PubMed: 23542691]
38. Michaud M, Martins I, Sukkurwala AQ, Adjemian S, Ma Y, Pellegatti P, Shen S, Kepp O, Scoazec M, Mignot G, Rello-Varona S, Tailler M, Menger L, Vacchelli E, Galluzzi L, Ghiringhelli F, di Virgilio F, Zitvogel L, Kroemer G. Autophagy-dependent anticancer immune responses induced by chemotherapeutic agents in mice. Science. 2011; 334:1573–1577. [PubMed: 22174255]
39. Schumacher TN, Schreiber RD. Neoantigens in cancer immunotherapy. Science. 2015; 348:69–74. [PubMed: 25838375]
40. Wang W, Kryczek I, Dostál L, Lin H, Tan L, Zhao L, Lu F, Wei S, Maj T, Peng D, He G, Vatan L, Szeliga W, Kuick R, Kotarski J, Tarkowski R, Dou Y, Rattan R, Munkarah A, Liu JR, Zou W. Effector T cells abrogate stroma-mediated chemoresistance in ovarian cancer. Cell. 2016; 165:1092–1105. [PubMed: 27133165]
41. Zou W, Wolchok JD, Chen L. PD-L1 (B7-H1) and PD-1 pathway blockade for cancer therapy: Mechanisms, response biomarkers, and combinations. Sci. Transl. Med. 2016; 8:328rv4.

42. Martinou J-C, Youle RJ. Mitochondria in apoptosis: Bcl-2 family members and mitochondrial dynamics. Dev. Cell. 2011; 21:92–101. [PubMed: 21763611]
43. O'Carroll D, Mecklenbrauker I, Das PP, Santana A, Koenig U, Enright AJ, Miska EA, Tarakhovsky A. A Slicer-independent role for Argonaute 2 in hematopoiesis and the microRNA pathway. Genes Dev. 2007; 21:1999–2004. [PubMed: 17626790]
44. DeBerardinis RJ, Chandel NS. Fundamentals of cancer metabolism. Sci. Adv. 2016; 2:e1600200. [PubMed: 27386546]
45. Brand A, Singer K, Koehl GE, Kolitzus M, Schoenhammer G, Thiel A, Matos C, Bruss C, Klobuch S, Peter K, Kastenberger M, Bogdan C, Schleicher U, Mackensen A, Ullrich E, Fichtner-Feigl S, Kesselring R, Mack M, Ritter U, Schmid M, Blank C, Dettmer K, Oefner PJ, Hoffmann P, Walenta S, Geissler EK, Pouyssegur J, Villunger A, Steven A, Seliger B, Schreml S, Haferkamp S, Kohl E, Karrer S, Berneburg M, Herr W, Mueller-Klieser W, Renner K, Kreutz M. LDHA-associated lactic acid production blunts tumor immunosurveillance by T and NK cells. Cell Metab. 2016; 24:657–671. [PubMed: 27641098]
46. Chang C-H, Curtis JD, Maggi LB Jr, Faubert B, Villarino AV, O'Sullivan D, Huang SC-C, van der Windt GJW, Blagih J, Qiu J, Weber JD, Pearce EJ, Jones RG, Pearce EL. Posttranscriptional control of T cell effector function by aerobic glycolysis. Cell. 2013; 153:1239–1251. [PubMed: 23746840]
47. Xu Y, Chaudhury A, Zhang M, Savoldo B, Metelitsa LS, Rodgers J, Yustein JT, Neilson JR, Dotti G. Glycolysis determines dichotomous regulation of T cell subsets in hypoxia. J. Clin. Invest. 2016; 126:2678–2688. [PubMed: 27294526]
48. Bonafé N, Gilmore-Hebert M, Folk NL, Azodi M, Zhou Y, Chambers SK. Glyceraldehyde-3-phosphate dehydrogenase binds to the AU-Rich 3' untranslated region of colony-stimulating factor–1 (CSF-1) messenger RNA in human ovarian cancer cells: Possible role in CSF-1 posttranscriptional regulation and tumor phenotype. Cancer Res. 2005; 65:3762–3771. [PubMed: 15867372]
49. Curiel TJ, Wei S, Dong H, Alvarez X, Cheng P, Mottram P, Krzysiek R, Knutson KL, Daniel B, Zimmermann MC, David O, Burow M, Gordon A, Dhurandhar N, Myers L, Berggren R, Hemminki A, Alvarez RD, Emilie D, Curiel DT, Chen L, Zou W. Blockade of B7-H1 improves myeloid dendritic cell–mediated antitumor immunity. Nat. Med. 2003; 9:562–567. [PubMed: 12704383]
50. Curiel TJ, Coukos G, Zou L, Alvarez X, Cheng P, Mottram P, Evdemon-Hogan M, Conejo-Garcia JR, Zhang L, Burow M, Zhu Y, Wei S, Kryczek I, Daniel B, Gordon A, Myers L, Lackner A, Disis ML, Knutson KL, Chen L, Zou W. Specific recruitment of regulatory T cells in ovarian carcinoma fosters immune privilege and predicts reduced survival. Nat. Med. 2004; 10:942–949. [PubMed: 15322536]
51. Cui TX, Kryczek I, Zhao L, Zhao E, Kuick R, Roh MH, Vatan L, Szeliga W, Mao Y, Thomas DG, Kotarski J, Tarkowski R, Wicha M, Cho K, Giordano T, Liu R, Zou W. Myeloid-derived suppressor cells enhance stemness of cancer cells by inducing microRNA101 and suppressing the corepressor CtBP2. Immunity. 2013; 39:611–621. [PubMed: 24012420]
52. Peng D, Kryczek I, Nagarsheth N, Zhao L, Wei S, Wang W, Sun Y, Zhao E, Vatan L, Szeliga W, Kotarski J, Tarkowski R, Dou Y, Cho K, Hensley-Alford S, Munkarah A, Liu R, Zou W. Epigenetic silencing of T_H1-type chemokines shapes tumour immunity and immunotherapy. Nature. 2015; 527:249–253. [PubMed: 26503055]
53. Gan B, Peng X, Nagy T, Alcaraz A, Gu H. Guan, Role of FIP200 in cardiac and liver development and its regulation of TNFα and TSC–mTOR signaling pathways. J. Cell Biol. 2006; 175:121–133. [PubMed: 17015619]
54. Sentman CL, Shutter JR, Hockenbery D, Kanagawa O, Korsmeyer SJ. bcl-2 inhibits multiple forms of apoptosis but not negative selection in thymocytes. Cell. 1991; 67:879–888. [PubMed: 1835668]

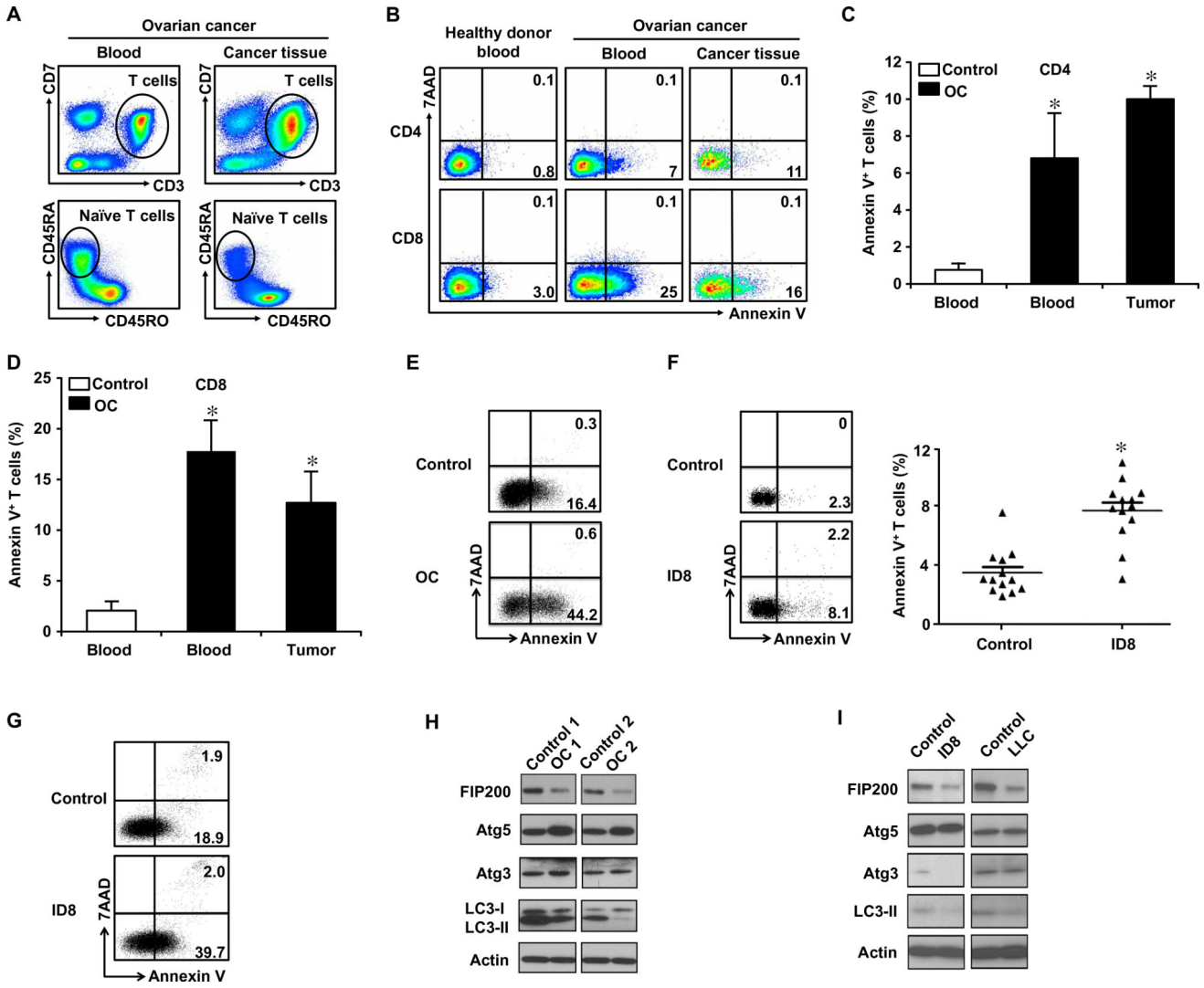

Fig. 1. FIP200 loss links to poor autophagy and high apoptosis in naïve T cells in tumor

(**A**) Phenotype of naïve T cells in blood and cancer tissues in ovarian cancer (OC) patients. Peripheral blood mononuclear cells and ovarian cancer tissue single cells were stained with antibodies against CD3, CD7, CD45RA, and CD45RO and analyzed with LSR II ($n = 5$). (**B** to **E**) Apoptotic naïve T cells in peripheral blood and ovarian cancer tissues in ovarian cancer patients. (B) Numbers on the dot plots represent the percentage of AnnexinV $^{+}$CD45RA^{+}CD45RO^{-}CD3^{+} naïve T cells. The percentages of Annexin V^{+}CD4^{+} (C) and Annexin V^{+}CD8^{+} (D) naïve T cells are shown ($n = 5$, means ± SEM). *$P < 0.05$ (Mann-Whitney U tests) compared with control group. (E) Human naïve T cells were cultured with anti-CD3 and anti-CD28 antibodies for 48 hours. Numbers on the dot plots represent the percentage of Annexin V^{+} T cells of activated naïve T cells ($n = 5$). (**F** and **G**) Apoptotic naïve T cells in healthy mice and ID8 tumor–bearing mice. (F) Numbers on the dot plots represent the percentage of Annexin V^{+}CD44^{-}CD3^{+} fresh naïve T cells in mesenteric lymph nodes ($n = 13$, means ± SEM). *$P < 0.05$ (Mann-Whitney U tests). (G) T cells were cultured with anti-CD3 and anti-CD28 antibodies for 48 hours. Numbers on the dot plots represent the percentage of Annexin V^{+} T cells of activated naïve T cells ($n = 7$). (**H**) Autophagy

component proteins in fresh peripheral blood naïve T cells in healthy human donors and ovarian cancer patients ($n = 6$). (**I**) Autophagy component proteins in fresh mouse naïve lymph node T cells from normal, ID8-, and LLC-bearing mice ($n = 3$).

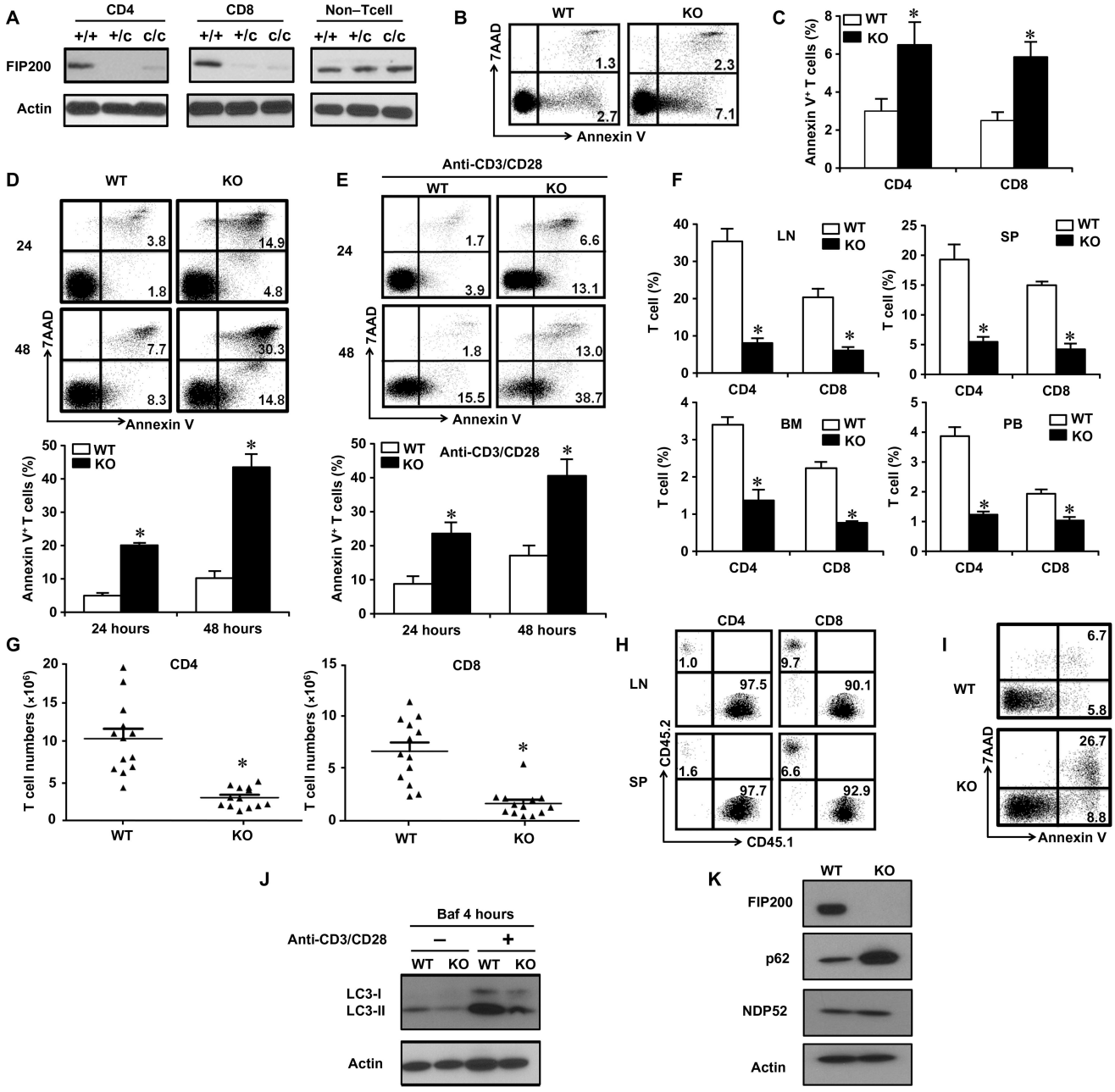

Fig. 2. Genetic FIP200 deletion impairs autophagy induction and causes T cell apoptosis

(**A**) FIP200 protein expression in T cell subsets and non–T cells from *Fip200*$^{flox/flox}$*Cd4*$^{+/+}$ (WT), *Cd4*$^{c/+}$, and *Cd4*$^{c/c}$ (KO) mice ($n = 3$). (**B** and **C**) Spontaneous apoptosis of naïve T cells in WT and *Fip200*$^{-/-}$ mice. (B) Numbers on the dot plots represent the percentage of Annexin V$^+$ naïve T cells in lymph nodes. (C) The percentages of CD4$^+$ and CD8$^+$ Annexin V$^+$ naïve T cells are shown ($n = 5$, means ± SEM). *$P < 0.05$ (Mann-Whitney *U* tests). (**D** and **E**) Apoptosis of cultured or activated T cells in WT and *Fip200*$^{-/-}$ mice. Naïve lymph node T cells were cultured for 24 and 48 hours without (D) or with (E) anti-CD3 and anti-CD28 antibodies. Numbers on the dot plots represent the percentage of Annexin V$^+$ T cells ($n = 4$, means ± SEM). *$P < 0.05$ (Mann-Whitney *U* tests). (**F**) The percentage of T cell

subsets in lymph nodes (LNs; $n = 6$), spleen (SP; $n = 5$ to 7), bone marrow (BM; $n = 3$), and peripheral blood (PB; $n = 3$) in WT and *Fip200*$^{-/-}$ mice. *$P < 0.05$ (Mann-Whitney U tests). (**G**) Absolute numbers of T cell subsets in spleen from WT and *Fip200*$^{-/-}$ mice ($n = 13$, means ± SEM). *$P < 0.05$ (Mann-Whitney U tests). (**H** and **I**) WT CD45.1^{+} T cells and *Fip200*$^{-/-}$ CD45.2^{+} T cells were transferred into *Rag1*$^{-/-}$ mice with a 1:1 ratio. Live (H) and apoptotic (I) T cells were analyzed on day 14 in the lymph nodes and spleen in *Rag1*$^{-/-}$ mice. Numbers on the dot plots represent the percentage of CD45.1^{+} and CD45.2^{+} T cells in total T cells (H) and the percentage of Annexin V^{+} T cells in WT and *Fip200*$^{-/-}$ (KO) T cells (I) ($n = 7$). (**J**) Autophagy flux in T cells isolated from lymph nodes of WT and KO mice with or without TCR engagement for 24 hours. These T cells were treated with Baf for the last 4 hours to inhibit the autophagosome degradation ($n = 3$). (**K**) Expression of autophagy receptor p62 and NDP52 in fresh WT and *Fip200*$^{-/-}$ naïve T cell subsets ($n = 3$).

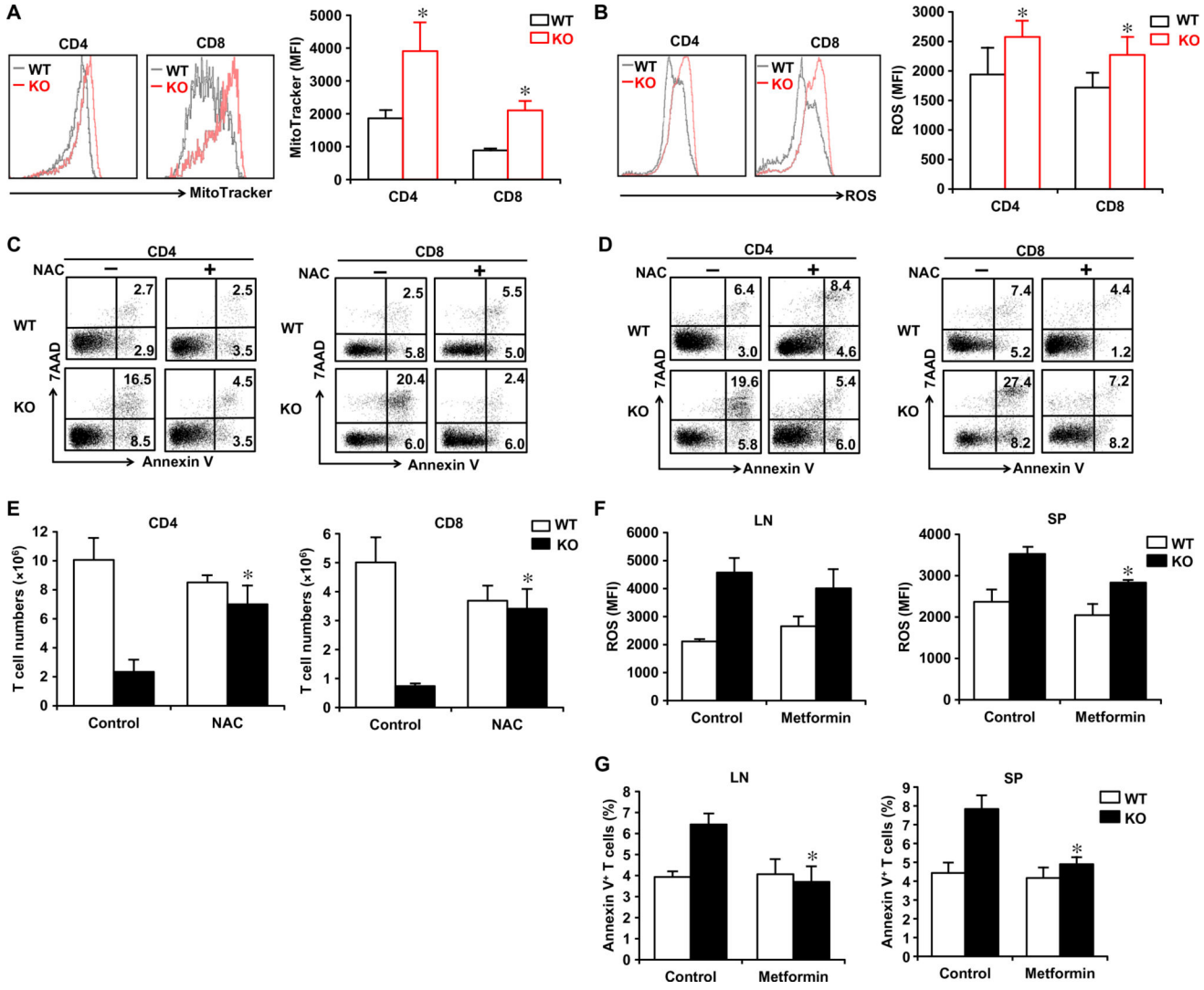

Fig. 3.

FIP200 deficiency alters mitochondria activation and ROS produc- G tion in T cells. (**A** and **B**) The mitochondria contents (A) and ROS production (B) were analyzed by FACS in naïve T cell subsets in WT and *Fip200*$^{-/-}$ mice ($n = 4$ to 5, means ± SEM). *$P < 0.05$ (Mann-Whitney U tests). MFI, mean fluorescence intensity. (**C**) Effects of NAC on WT and *Fip200*$^{-/-}$ T cell apoptosis in vitro. T cell subsets were treated with 0.1 mM NAC for 12 hours. Numbers on the dot plots represent the percentage of Annexin V$^+$ T cells ($n = 3$). (**D** and **E**) Effects of NAC on WT and *Fip200*$^{-/-}$ T cell apoptosis in vivo. Mice were treated daily with NAC for 4 weeks. (D) Apoptosis was determined by Annexin V staining in activated T cells. (E) The absolute numbers of naïve CD4$^+$ and CD8$^+$ T cells were quantified in lymph nodes in WT and *Fip200*$^{-/-}$ mice without or with NAC treatment ($n = 4$ to 5, means ± SEM). *$P < 0.05$ (Mann-Whitney U tests) between KO mice without and with NAC treatment. (**F** and **G**) Effects of metformin on WT and *Fip200*$^{-/-}$ naïve T cell ROS and apoptosis in vivo. Mice were treated daily with metformin for 2 weeks. (F) The ROS production was analyzed by FACS in naïve T cell subsets in WT and *Fip200*$^{-/-}$ mice. (G) The percentage of Annexin V$^+$ T cells in lymph node and spleen from WT and *Fip200*$^{-/-}$

mice ($n = 3$, means ± SEM). *$P < 0.05$ (Mann-Whitney U tests) between KO mice without and with metformin treatment.

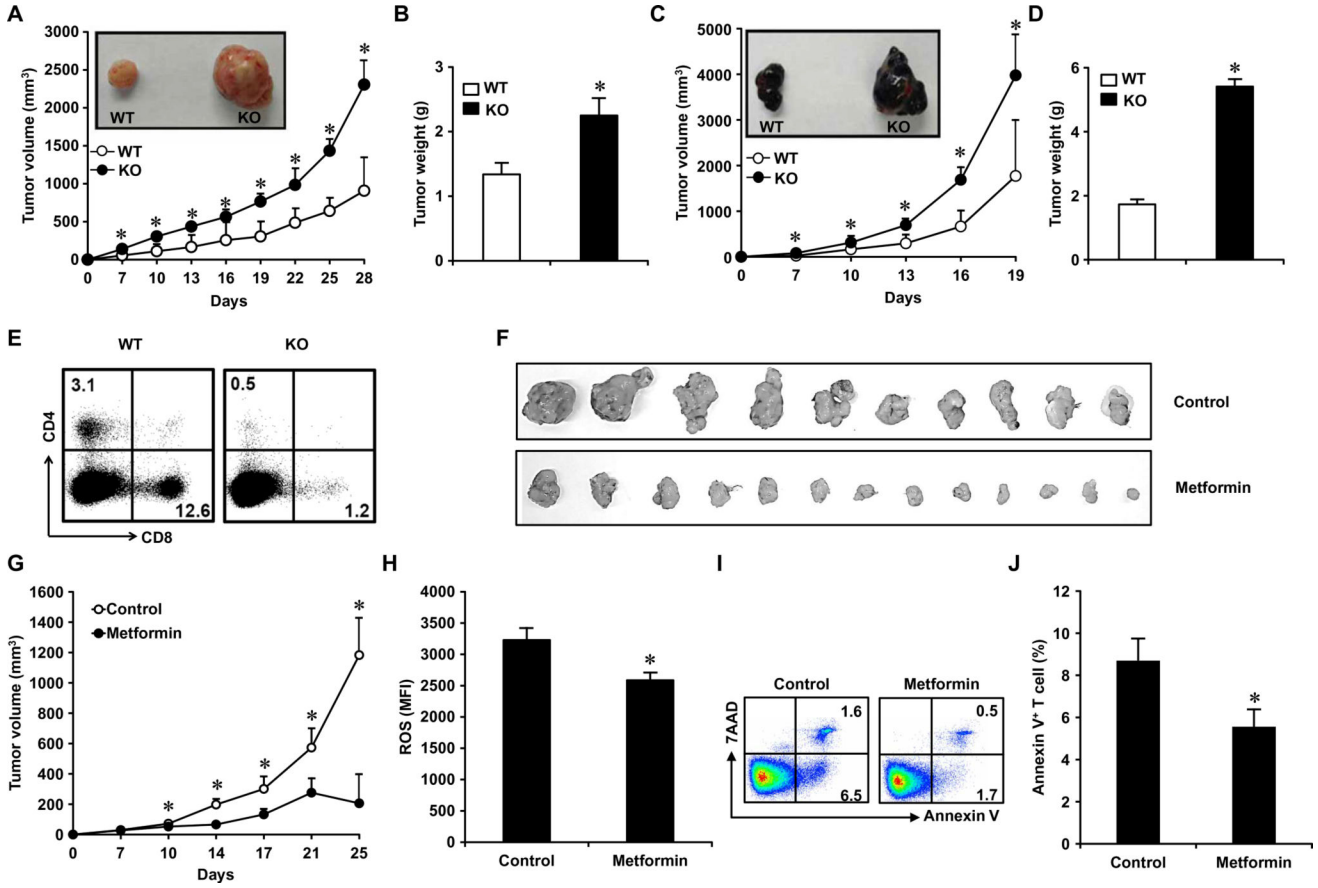

Fig. 4. Impaired antitumor immunity in *Fip200*$^{-/-}$ mice

(**A** to **D**) Effect of T cell FIP200 deficiency on tumor growth in vivo. MC38 (A and B) and B16 cells (C and D) were subcutaneously inoculated into WT and *Fip200*$^{-/-}$ mice. Tumor volume (A and C) was monitored, and tumor weight (B and D) was recorded at the end of the experiments ($n = 5$, means ± SEM). *$P < 0.05$ (Mann-Whitney U tests) between WT and *Fip200*$^{-/-}$ tumor size at the indicated time. (**E**) Effect of T cell FIP200 deficiency on T cell tumor infiltration. CD4$^+$ and CD8$^+$ cells were analyzed by FACS in MC38 tumor tissues. Numbers on the dot plots represent the percentage of CD4$^+$ and CD8$^+$ T cells in CD45$^+$ cells ($n = 3$). (**F** and **G**) Effect of metformin on MC38 tumor growth in vivo. MC38-bearing mice were treated with metformin or control for 18 days from day 7. Tumor images (F) and volume (G) are shown ($n = 14$ to 15, means ± SEM). *$P < 0.05$ (Mann-Whitney U tests). (**H**) Effect of metformin on ROS production in naïve T cell in MC38-bearing mice treated with metformin and control ($n = 5$, means ± SEM). *$P < 0.05$ (Mann-Whitney U tests). (**I** and **J**) Effect of metformin on naïve T cell apoptosis in MC38-bearing mice treated with metformin and control. (I) Numbers on the dot plots represent the percentage of Annexin V $^+$CD44$^-$CD3$^+$CD62L$^+$ naïve T cells ($n = 5$). (J) The percentages of Annexin V $^+$CD44$^-$CD3$^+$CD62L$^+$ naïve T cells are shown ($n = 5$, means ± SEM). *$P < 0.05$ (Mann-Whitney U tests).

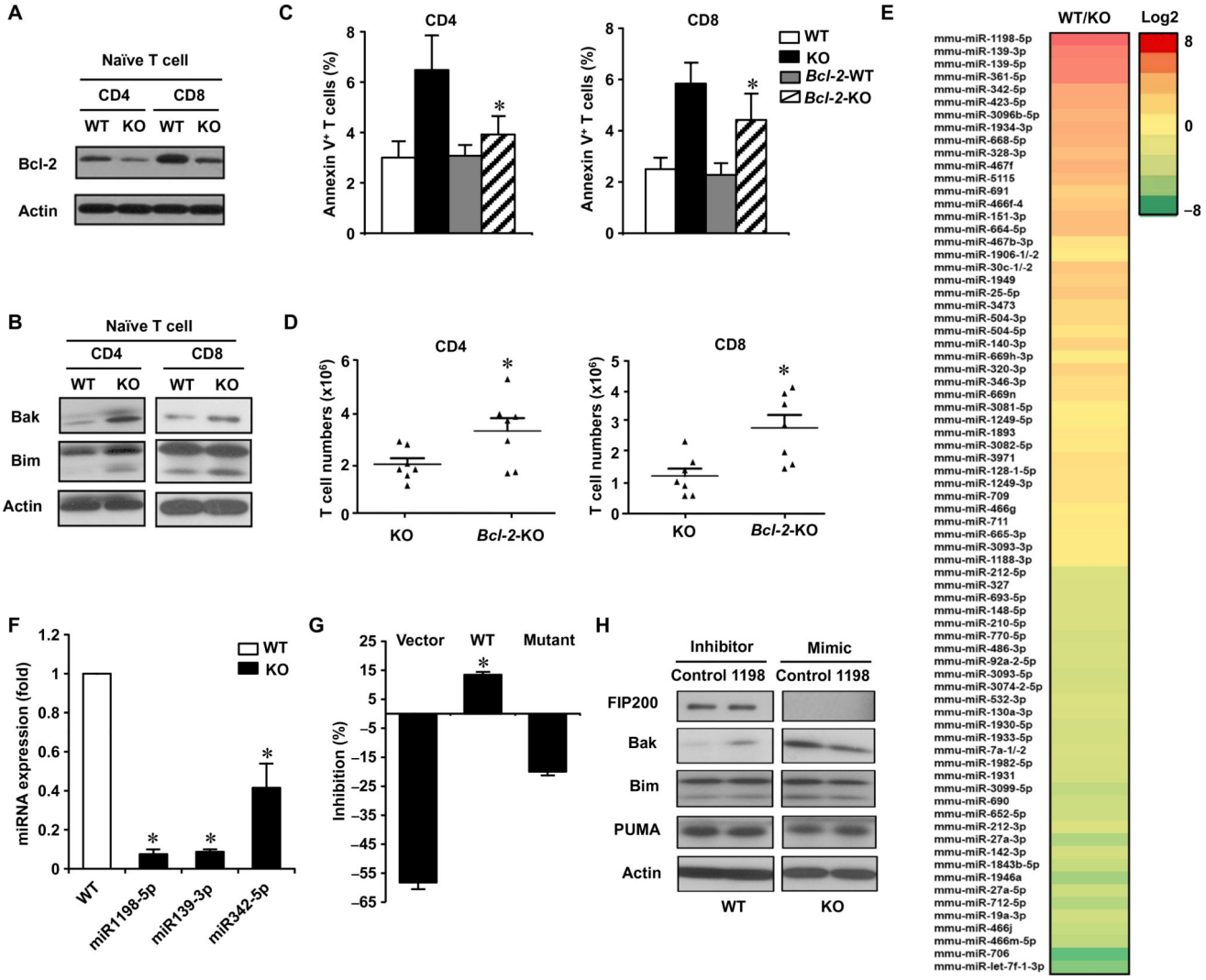

Fig. 5. FIP200 controls Bak expression via maintaining microRNA1198-5p expression

(**A**) Bcl-2 protein was detected in T cell subsets in WT and *Fip200*$^{-/-}$ mice ($n = 3$). (**B**) Bak and Bim proteins were detected in T cell subsets in WT and *Fip200*$^{-/-}$ mice ($n = 3$). (**C**) T cell apoptosis in WT, *Fip200*$^{-/-}$, *Bcl-2* transgenic (*Bcl-2*–WT) and *Fip200*$^{-/-}$ *Bcl-2* transgenic mice (*Bcl-2*–KO; $n = 3$ to 5, means ± SEM). *$P < 0.05$ between KO and *Bcl-2*–KO (Mann-Whitney *U* tests). (**D**) Absolute numbers of T cell subsets in *Fip200*$^{-/-}$ and *Bcl-2*–KO spleen ($n = 7$, means ± SEM). *$P < 0.05$ (Mann-Whitney *U* tests). (**E**) Heat map of microRNAs in *Fip200*$^{-/-}$ naïve CD4$^+$ T cells. MicroRNA arrays of naïve CD4$^+$ T cells in WT and *Fip200*$^{-/-}$ mice. A fold change of >0.25 is shown. The red color represents high levels of microRNA expression in WT naïve CD4$^+$ T cells as compared with *Fip200*$^{-/-}$ naïve CD4$^+$ T cells. (**F**) Expression of three microRNAs in *Fip200*$^{-/-}$ naïve CD4$^+$ T cells ($n = 4$, means ± SEM). *$P < 0.05$ (Mann-Whitney *U* tests). (**G**) Effect of microRNA1198-5p mimics on WT 3′UTR-*Bak1* luciferase activity. The luciferase activity was measured in 293FT cells transfected with WT or mutant 3′UTR sequence of *Bak1* ($n = 3$ in triplicate, means ± SEM). *$P < 0.05$ between WT and mutant (Student's *t* tests). (**H**) Effects of microRNA1198-5p inhibitors and mimics on proapoptotic gene expression. WT and

Fip200$^{-/-}$ T cells from lymph nodes were transfected with microRNA1198-5p inhibitors or mimics for 48 hours. Proapoptotic proteins were detected by Western blotting ($n = 3$).

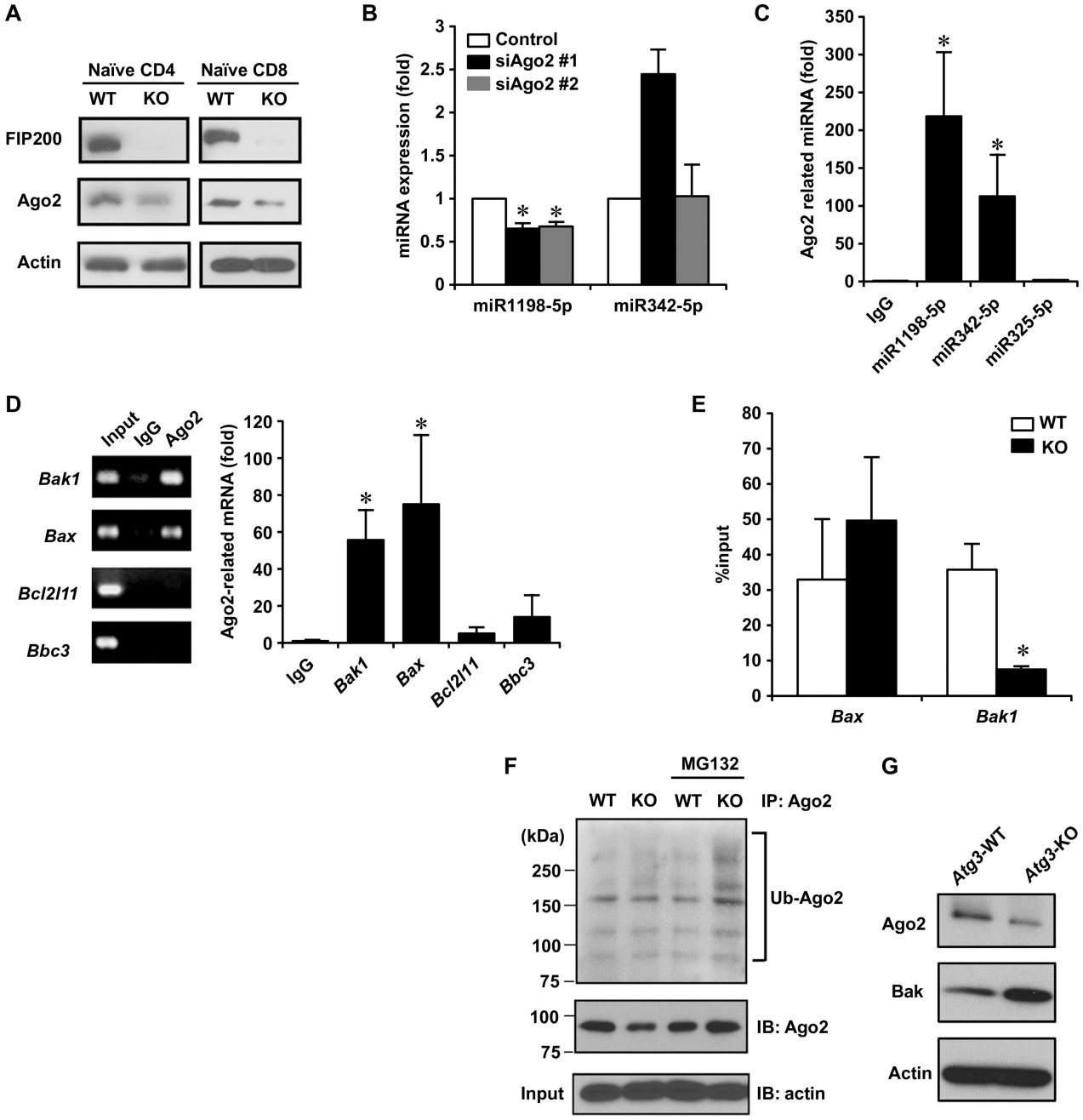

Fig. 6. FIP200 maintains microRNA1198-5p expression via Ago2 in naïve T cells

(**A**) Expression of Ago2 protein in WT and *Fip200*$^{-/-}$ naïve T cells ($n = 3$). (**B**) Effect of Ago2 siRNAs on microRNA1198-5p expression. WT naïve CD4^{+} T cells were transfected with Ago2 siRNAs (#1 and #2) for 48 hours. The expression of micorRNA1198-5p and microRNA342-5p was quantified by real-time PCR ($n = 3$ to 5, means ± SEM). *$P < 0.05$ (Student's *t* tests). (**C** and **D**) Expression of microRNA1198-5p (C) and *Bak1* mRNA (D) in the Ago2 complex ($n = 3$, means ± SEM). *$P < 0.05$ (Student's *t* tests). (**E**) Contents of *Bak1* and *Bax* mRNAs in the Ago2 complex in WT and *Fip200*$^{-/-}$ naïve T cells. The data are shown as the percentage of *Bak1* and *Bax* mRNA expression compared with input ($n =$

3, means ± SEM). *$P < 0.05$ of *Bak1* expression between WT and *Fip200*$^{-/-}$ T cells (Mann-Whitney *U* tests). (**F**) Ago2 ubiquitination in WT and *Fip200*$^{-/-}$ naïve T cells. Naïve T cells were treated with or without proteasome inhibitor MG132 (10 μM) for 2 hours ($n = 3$). IP, immunoprecipitation; IB, immunoblotting. (**G**) Expression of Ago2 and Bak protein in *Atg3*-WT and *Atg3*-KO naïve T cells ($n = 3$).

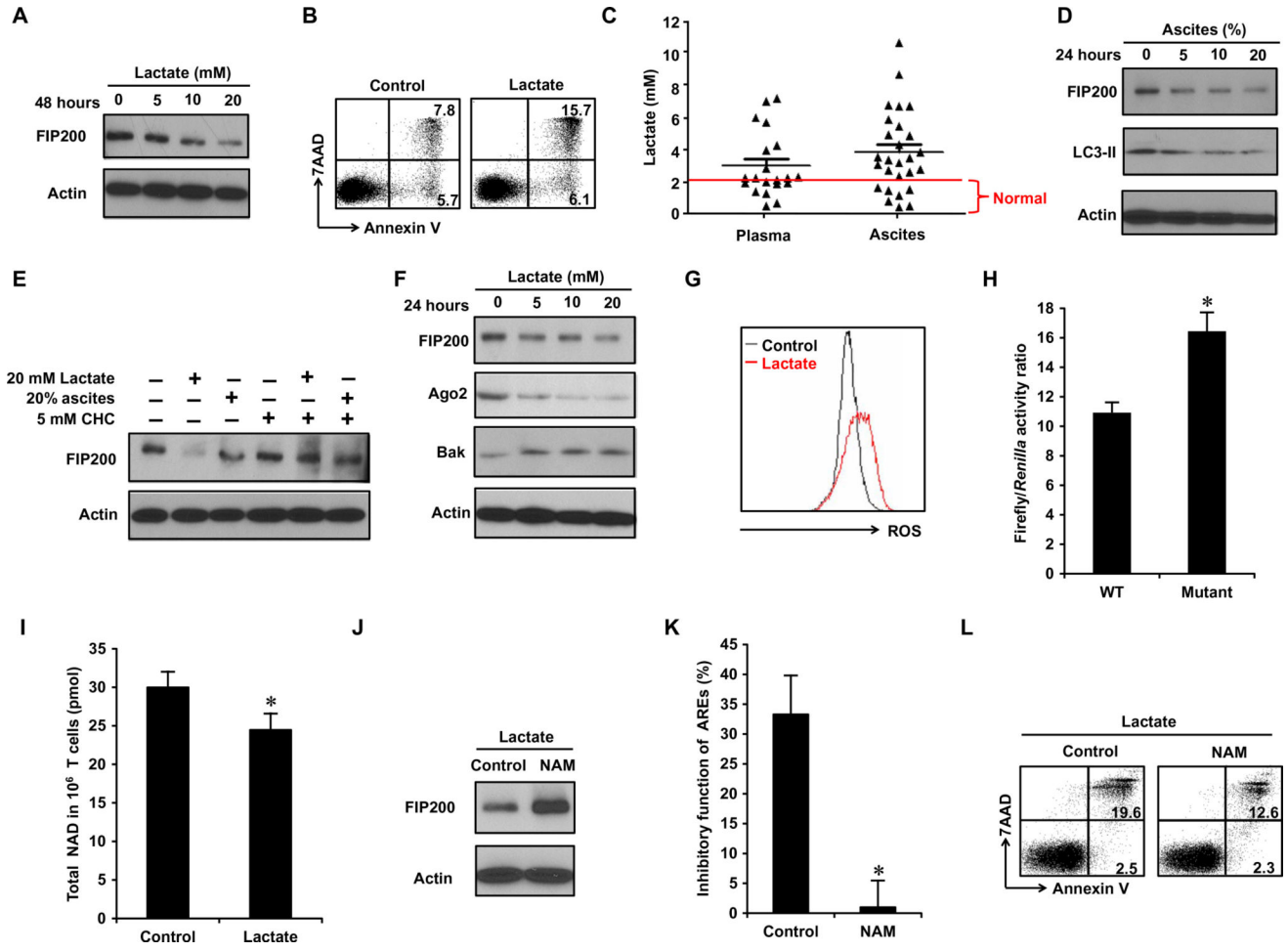

Fig. 7. Tumor-derived lactate suppresses FIP200 expression in naïve T cells

(**A**) Effect of lactate on FIP200 protein expression in human naïve T cells treated with lactate for 48 hours ($n = 3$). (**B**) Effect of lactate on human naïve T cells apoptosis treated with 20 mM lactate for 48 hours. Numbers on the dot plots represent the percentage of Annexin V^+ naïve T cells ($n = 3$). (**C**) Lactate levels in the plasma and ascites of ovarian cancer patients. Lactate concentrations were measured in 20 plasma samples and 27 ascites. The normal range of lactate plasma levels determined in healthy individuals (0 to 2.2 mM) is indicated below the red line. (**D**) Effect of ascites on FIP200 and LC3-II protein in human naïve T cells treated with ascites for 24 hours ($n = 3$). (**E**) Effect of CHC on the role of lactate and ascites in FIP200 expression in human naïve T cells treated with different conditions for 48 hours ($n = 3$). (**F**) Effect of lactate on FIP200, Ago2, and Bak protein expression in mouse naïve T cells treated with different conditions for 24 hours in the presence of interleukin-7 (IL-7; $n = 3$). (**G**) Effect of lactate on ROS expression in mouse naïve T cells treated with 20 mM lactate for 48 hours with IL-7 ($n = 3$). (**H**) Effect of AREs in 3′UTR-*Fip200* on luciferase activity. The luciferase activity was measured in 293FT cells transfected with WT or mutant mouse *Fip200* 3′UTR vectors for 48 hours. ($n = 3$ in triplicate, means ± SEM). *$P < 0.05$ between WT and mutant (Student's *t* tests). (**I**) Effect of lactate on NAD level in mouse naïve T cells treated with 20 mM lactate for 24 hours. The

total NAD in 10^6 T cells was measured ($n = 5$, means ± SEM). *$P < 0.05$ between control and lactate treatment (Student's t tests). (**J**) Effect of lactate on FIP200 expression in mouse naïve T cells treated with 20 mM lactate in the presence of 5 mM NAM for 24 hours ($n = 3$). (**K**) Effect of NAM on the inhibitory role of the AREs in 3′UTR-*Fip200*. 293FT cells were transfected with mouse WT or mutant 3′UTR-*Fip200* plasmids for 24 hours and were treated with NAM for an additional 24 hours. Results are shown as the decreased percentage of WT luciferase activity to that of the mutant [(mutant luciferase − WT luciferase)/mutant luciferase] ($n = 3$ in triplicate, means ± SEM). *$P < 0.05$ between control and NAM treatment (Student's t tests). (**L**) Effect of NAM on naïve T cell apoptosis induced by lactate. Mouse naïve T cells were treated with lactate in the presence of NAM for 24 hours. Numbers on the dot plots represent the percentage of Annexin V^+ naïve T cells ($n = 3$).